Original Article

pISSN, eISSN 0125-5614
M Dent J 2025; 45 (2) : 109-122

ResNet-18 architecture for multi-label classification of alveolar antral artery canal positions in coronal cone-beam computed tomography images with threshold optimization

Thachamon Mepetch[1], Suchaya Pornprasertsuk-Damrongsri[2], Akara Supratak[3], Suraphong Yuma[4], Sarunya Chaikantha[2], **Chakorn Vorakulpipat**[5]

[1] *Master of Science Program in Oral and Maxillofacial Surgery, Faculty of Dentistry, Mahidol University, Bangkok, Thailand*
[2] *Department of Oral and Maxillofacial Radiology, Faculty of Dentistry, Mahidol University, Phayathai Campus, Bangkok, Thailand*
[3] *Faculty of Information and Communication Technology, Mahidol University, Salaya Campus, Nakorn Pathom, Thailand*
[4] *Department of Physics, Faculty of Science, Mahidol University, Bangkok, Thailand*
[5] *Department of Oral and Maxillofacial Surgery, Faculty of Dentistry, Mahidol University, Phayathai Campus, Bangkok, Thailand*

Objectives: The alveolar antral artery (AAA) supplies the posterior maxillary region. Detecting this artery using radiographs is essential before oral and maxillofacial surgeries to prevent bleeding complications. However, manual radiograph interpretation is time-consuming and requires expert experience. This study aims to develop and evaluate a ResNet-18 deep learning model that applies varying thresholds for multi-label classification of the AAA canal positions categorized as intraosseous, superficial, or intrasinus in coronal cone-beam computed tomography (CBCT) images.

Materials and Methods: Coronal CBCT images of 60 patients were selected and categorized into training data and testing data. Annotation of the AAA canal positions was done by experts via the Computer Vision Annotation Tool. Image transformation and augmentation techniques were applied to optimize a model training. A ResNet-18 model was trained with five-fold cross-validation. The best-performing model for each fold was determined based on the F1- score of the validation and tested on the test set.

Results: The model achieved a micro F1-score of 0.8206 when applying class-specific thresholds of 0.411, 0.452, and 0.515 for the superficial, intrasinus, and intraosseous positions, respectively. A single threshold of 0.452 and 0.500 marginally decreased the micro F1-scores to 0.8193 and 0.8157, respectively. The class-specific thresholds strategy yielded the highest per-class F1-scores, with values of 0.8153 for intraosseous, 0.6470 for intrasinus, and 0.0164 for the superficial class.

Conclusions: The implementation of deep learning for the AAA canal classification aids dentists and oral surgeons in preoperative planning, minimizing iatrogenic injury of the artery during surgery. Additionally, knowing the artery's position beforehand enhances perioperative and postoperative management, allowing for better handling of complications in the event of vascular injury, potentially improving surgical outcomes and reducing procedural complications, benefiting both clinicians and patients.

Keywords: alveolar antral artery, artery, cone-beam computed tomography, convolutional neural networks, deep learning, sinus lift

How to cite: Mepetch T, Pornprasertsuk-Damrongsri S, Supratak A, Yuma S, Chaikantha S, **Vorakulpipat C**. ResNet-18 architecture for multi-label classification of alveolar antral artery canal positions in coronal cone-beam computed tomography images with threshold optimization. M Dent J 2025;45(2): 109-122.

Corresponding author: Chakorn Vorakulpipat
Department of Oral and Maxillofacial Surgery, Faculty of Dentistry, Mahidol University,
6 Yothi Road, Ratchathewi, Bangkok 10400, Thailand
Tel: + 66 2200-7845 Email: chakorn.vor@mahidol.ac.th
Received: 28 March 2025 **Revised:** 7 May 2025 **Accepted:** 21 May 2025

Introduction

Dental implant placement is an oral surgical procedure utilized to replace the edentulous region. A significant challenge in dental implant placement in the posterior maxilla is insufficient alveolar bone height, often presenting as an atrophic condition [1]. Currently, the sinus lift procedure is among the most commonly employed surgical interventions to address this issue. The fundamental approach involves creating an osteotomy to establish a window in the lateral wall of the maxillary sinus. The sinus membrane is then elevated to create a space beneath it, which is subsequently filled with grafting materials. This technique ensures the augmentation of bone height, facilitating the placement of osseointegrated implants [2].

The alveolar antral artery (AAA) is a significant vascular structure that courses through the anterolateral wall of the maxillary sinus, providing essential blood supply to the lateral wall of the maxillary sinus, Schneiderian membrane, periosteal tissues, and posterior maxillary teeth [3]. It is formed by anastomosis between the posterior superior alveolar artery (PSAA) and the infraorbital artery (IOA) [4]. The AAA canal is anatomically located in three mediolateral positions, including intraosseous (within the lateral sinus wall), intrasinus (beneath the sinus membrane), and superficial (under the periosteum). Among these, the intrasinus and intraosseous positions are the most prevalent [5, 6].

Iatrogenic injury to the AAA canal during sinus lift procedures can result in significant intraoperative and postoperative bleeding and subsequent complications. The study of Zijderveld *et al* [7] in 2008 reported that 2% of the cases experienced intraoperative bleeding from this artery during sinus lift. The presence of bleeding impaired visualization and made the surgical procedure more challenging. Another case report also found that bleeding can persist in the immediate postoperative period or be delayed for up to seven hours after surgery representing ongoing bleeding and progressive swelling a few hours after a transcrestal sinus lift, presumably from a lacerated of the AAA canal by an osteotomy path close to the lateral sinus wall [8]. While hemorrhage from this vessel rarely presents life-threatening scenarios, it introduces critical surgical challenges, including impaired field visualization, extended operative time, loss of graft materials, and sinus membrane perforation, potentially leading to hemosinus and sinus dysfunction [9, 10].

Since each positional variation of the AAA canal significantly influences surgical planning and requires different technique selection, precise preoperative classification and evaluation of the artery canal positions enable surgeons to tailor their interventions, ensuring optimal procedural outcomes while minimizing the risk of vascular injury and associated adverse events [11]. For instance, if the artery is located superficially, surgeons can carefully detach the vessel from the bone and reflect with the buccal flap without damaging it. However, if it is intraosseous, the recommendation is to avoid its course by modifying the size and position of the osteotomy such as a double-window technique. In cases where the artery is intrasinus, the surgeons can either carefully detach and reflect the artery along with the sinus membrane or change the area of the approach. Also, piezoelectric devices may be utilized to create a bony window without compromising the membrane or vessel, allowing the artery to move upward with the sinus membrane [2, 9].

Among various imaging modalities, CBCT is considered the current method for the AAA canal detection, with identification rates of 60.3% to 94.6% [5, 12, 13], significantly higher than conventional computed tomography (CCT) 42-60%, and panoramic radiographs 1% [14]. While the detection of the AAA canal varies

across imaging techniques, cadaveric studies consistently reported the presence of the AAA in all investigations [3, 15, 16]. However, CBCT interpretation has limitations, including time-consuming, requiring experience, resolution constraints, and the possibility of false negatives due to small vessel diameter or anatomical variations [10].

Recent advancements in artificial intelligence (AI), particularly deep learning (DL), have significantly enhanced medical image processing by addressing limitations of traditional diagnostic approaches. Convolutional neural networks (CNNs), a subset of DL, are particularly effective in tasks such as image classification, object detection, and segmentation due to their ability to automatically extract and learn relevant features from pixel-level data [17, 18]. In this study, which focuses on multi-label classification of the anatomical position of the AAA canal from CBCT images, the ResNet-18 model was selected. The ResNet-18 offers an optimal balance between performance and efficiency, making it well-suited for small and imbalanced medical datasets [19]. Originally proposed by He *et al* [20] in 2015, ResNet employs residual connections to facilitate gradient flow, addressing vanishing gradient issues and enabling stable training of deeper networks. Compared to deeper variants such as ResNet-50, DenseNet, or Inception-v4, the ResNet-18 achieves competitive performance while requiring fewer computational resources and outperforms deeper models in classifying lung images of COVID-19 patients from computed tomography (CT) scans [21]. This makes it particularly advantageous for clinical environments where resources may be limited and highlights its robustness on small or noisy datasets. Although newer architectures such as DenseNet or EfficientNet can achieve high accuracy, they typically require significantly more computing resources and longer training times [21, 22]. In direct comparisons within medical imaging, ResNet-18 has consistently shown strong performance while being simpler to train and more practical for clinical use [23], making it particularly suitable for this study.

In dental imaging, CNNs have demonstrated utility in detecting key anatomical structures, including the maxillary sinus, tongue, and mandibular canals, thereby supporting improved diagnosis and treatment planning [24-27]. With regard to the AAA canal, numerous studies have extensively documented its anatomical characteristics, such as prevalence, diameter, position, and location using conventional methods [5, 12, 28, 29]. Existing studies primarily apply a deep learning to focus on identifying the location of the AAA canal in individual CBCT slices [30]. However, manual inspection is still required to further classify it into superficial, intraosseous, or intrasinus categories. Additionally, the performance of these techniques remains uncertain in cases where the AAA is absent or when multiple AAAs appear within a single slice. To overcome these limitations, this study proposes an automated classification model using ResNet-18 with a threshold-based approach to classify the AAA canal positional variants in coronal CBCT images. The proposed approach effectively handles cases where the AAA is absent or multiple AAAs appear within a single slice, reducing the need for manual inspection by automating the classification process.

Materials and Methods

Ethical Criteria

This retrospective study utilized existing radiographic data for classification purposes and was conducted collaboratively between the Department of Oral and Maxillofacial Radiology and Oral and Maxillofacial Surgery Clinic, Faculty of Dentistry, Mahidol University, Bangkok, and the Faculty of Information and Communication Technology,

Mahidol University, Nakhon Pathom, Thailand. The study protocol was in accordance with the ethical standards of the responsible committee on human experimentation (COA.No.MU-DT/PY-IRB 2024/004.1501) with the Declaration of Helsinki. A formal data-sharing agreement was established between the participating faculties. No additional imaging was performed specifically for this research. No experimental procedures were conducted on human subjects or tissues. All patient data were anonymized prior to analysis to ensure confidentiality and protection of patient privacy.

The overall workflow of this research is shown in Figure 1. Coronal CBCT images were retrospectively analyzed and annotated by expert clinicians to categorize multiple AAA canal positions. The annotated dataset was randomly divided into training and testing set. A ResNet-18 deep learning model was developed using five-fold cross-validation. Finally, model performance was assessed on the testing set using threshold-based classification, with the F1-score as the primary evaluation metric.

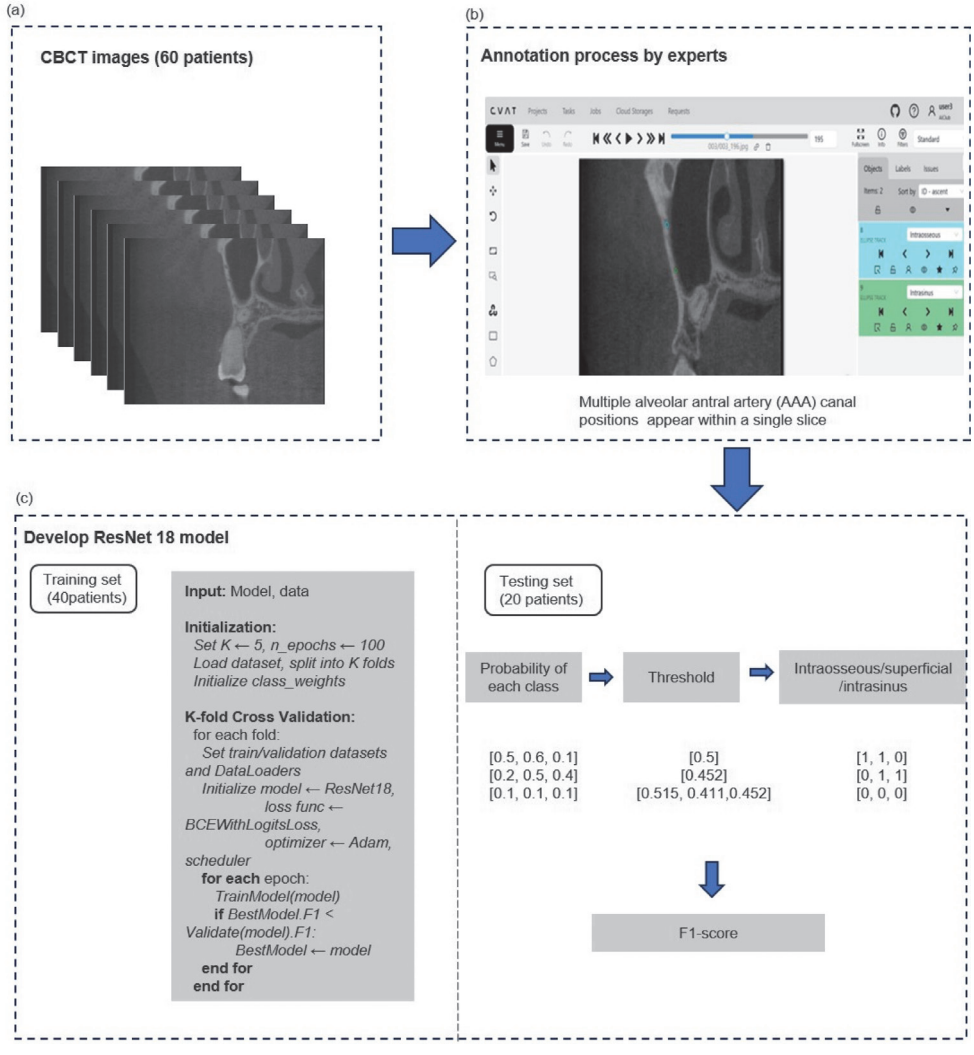

Figure 1 The overall workflow of this research in three main steps: (a) collection of coronal view of cone-beam computed tomography (CBCT) images. (b) expert annotators labeled AAA canal positions. (c) model development and evaluation.

Patient Selection and Data Collection

Coronal CBCT images from 60 patients (28 males, 32 females, with an age range of 19-68 years) who visited the Faculty of Dentistry, Mahidol University, between 2019 and 2020 for clinical purposes were retrospectively collected. Approximately 480 consecutive coronal slices of the maxillary region were extracted for each patient, resulting in a total dataset of 28,800 images. These consecutive slices ensured comprehensive anatomical coverage of the posterior maxilla, where the AAA canal typically courses. Image acquisition was performed using a 3D Accuitomo 170 Cone Beam Computed tomography machine (J. Morita CORP., Osaka, Japan) with the field of view (FOV) of 6 cm x 6 cm and voxel size of 125 μm. The inclusion criteria consisted of coronal CBCT images of patients aged over 18 years, acquired from the maxillary region, with adequate sharpness and diagnostic quality, regardless of the AAA visibility. Exclusion criteria included coronal CBCT images from patients with a history of jaw fracture, jaw surgery in the maxilla, craniofacial deformity, pathological conditions or diseases affecting the maxillary bone, insufficient image quality, such as blurred images, or excessive metal-induced or movement artifacts.

All coronal CBCT images were viewed on an Eizo RX 430 medical-grade monitor (Eizo Nanao Corp., Japan) with a resolution of 2560 x 1600 pixels using i-dixel software (J. Morita CORP., Osaka, Japan). Eligible datasets were anonymized and exported in Digital Imaging Communications in Medicine (DICOM) format via PLANMECA Romexis. These were subsequently converted to Joint Photographic Experts Group (JPEG) format using Fiji ImageJ software for further processing and analysis.

Ground-Truth Labeling

The dataset includes variations in which the AAA canal is either present or absent. When present, it is classified into one of three positional categories including intraosseous, intrasinus, or superficial, as illustrated in Figure 2. The dataset was uploaded to Computer Vision Annotation Tool (CVAT), an online platform for annotating visual data. Consensus-based interobserver agreement was performed in the study. The ground truth of the AAA canal positions was independently annotated by a postgraduate student, majoring in Oral and Maxillofacial surgery and by the 27 years' experience Oral and Maxillofacial radiologist. Any disagreements were resolved through discussion until a consensus was reached.

Figure 2 The classification of alveolar antral artery (AAA) positions in cone-beam computed tomography (CBCT) images. (a) intraosseous, (b) intrasinus, (c) superficial, and (d) absent of the artery.

Data Preprocessing and Characteristic

The data preprocessing process involved standardized image transformations and augmentation techniques to improve model training. Initially, all input images were resized to 224 × 224 pixels as per the model's requirements and converted to grayscale for consistency. Data augmentation techniques were applied, including horizontal flipping, minor rotational adjustments (1°), brightness and contrast modifications, and positional shifts using Affine Transform. These methods ensured an expanded dataset while maintaining the clinically significant features of AAA canal positions.

Model Training, Validation, and Testing

The total dataset consists of coronal CBCT scans from 60 patients were divided at the subject level into a training set (40 patients) and a test set (20 patients), ensuring that no images from the same patient appeared in both the training and test sets. Within the training set, the dataset was further split into five-fold cross-validation for a model training. The distribution of samples per class is presented in Table 1 including intraosseous (3,885 samples), superficial (301 samples), and intrasinus (3,079 samples). During cross-validation, the dataset was partitioned into five subsets, where in each fold, a different subset was used for validation while the remaining four subsets were used for training. A ResNet-18 model was employed as the base architecture for multi-label classification of the AAA canal positions. Formally, let there be m training examples:

$\{(X^{(1)}, Y^{(1)}),...,(X^{(i)}, Y^{(i)}),...,(X^{(m)}, Y^{(m)})\}$, where each $X^{(i)} \in \mathbb{R}^{224\times224}$ represents a single 224×224 CBCT image slice, and $Y^{(i)} = [Y_1^{(i)}, Y_2^{(i)}, Y_3^{(i)}]$ is a vector of ground truth labels. Each $Y_j^{(i)} \in \{0,1\}$ indicates the presence (1) or the absence (0) of the AAA position, where $j = 1, 2, 3$ corresponds to intraosseous, superficial, and intrasinus positions, respectively.

Table 1 Distribution of training data across five-folds

Fold \ Class	Intraosseous	Superficial	Intrasinus	Neither
1	1,200	152	1334	0
2	973	54	857	0
3	604	42	323	0
4	488	22	266	0
5	620	31	299	1
Total	3,885	301	3,079	1

The model predicts the probability of the AAA positions being present, producing an output vector: $\hat{Y}^{(i)} = [\hat{Y}_1^{(i)}, \hat{Y}_2^{(i)}, \hat{Y}_3^{(i)}]$, where $\hat{Y}_j^{(i)} \in [0,1]$ represents the predicted confidence score for the presence of the AAA position in class j. If $\hat{Y}_j^{(i)}$ exceeds a predefined threshold thd_j (i.e., $\hat{Y}_j^{(i)} \geq thd_j$), the model predicts that there is AAA position in class j. Our model was trained over 100 epochs. The binary cross-entropy with class weights were utilized as the loss function to address class imbalance. The optimization was employed using the Adam optimizer with a ReduceLROnPlateau learning rate scheduler. The best-performing model for each fold was determined based on the validation F1- score and subsequently saved for further evaluation. After training, each model was evaluated based on its performance on the validation set, and the model with the highest validation F1-score was selected for testing with the test set. During testing, different thresholding strategies were applied to improve multi-label classification performance. Initially, a single default threshold of 0.500 was used for all classes, but it was later uniformly lowered to 0.452 to address class imbalance and improve sensitivity for underrepresented classes. Additionally, a class-specific thresholding strategy was implemented to refine predictions based on the unique distribution of prediction scores for each class, setting thresholds at 0.515 for intraosseous, 0.411 for superficial, and 0.452 for intrasinus. Unlike a single-threshold approach, class-specific thresholds allow independent calibration for each class, accounting for differences in class prevalence and prediction score distributions. This method better addresses class imbalance by optimizing the trade-off between precision and recall for each class individually, thereby enhancing overall model performance.

Performance Evaluation

The model's performance was evaluated using the F1-score metric. The F1-score, calculated as the harmonic mean of precision and recall, was implemented at two levels of analysis.

$$\text{Precision} = \frac{TP}{TP+FP}$$

$$\text{Recall} = \frac{TP}{TP+FN}$$

The per-class F1-Score evaluates the performance of a model for each class representing intraosseous, superficial, and intrasinus by balancing precision and recall for that class.

$$\text{Per-class F1-Score} = 2 \times \frac{(Precision \times Recall)}{Precision+Recall}$$

The micro F1-Score evaluates the overall performance of the model by summing up true positives (TP), false positives (FP), and false negatives (FN) across all positions. True Positive (TP) represents instances where the model's classification aligned with expert assessment, while False Negative (FN) indicates cases where the model failed to detect an existing AAA canal feature category. False Positive (FP) denotes instances where the model incorrectly classified features as belonging to a particular category.

$$\text{Micro F1-Score} = \frac{2 \times Sum\ of\ TP}{2 \times Sum\ of\ TP+Sum\ of\ FP+Sum\ of\ FN}$$

Results

The performance of the ResNet-18 model using different threshold strategies was evaluated using per-class F1-scores and the overall micro-average F1-score. The per-class F1-scores reflect the model's performance for

each artery position when its respective threshold is applied, while the overall micro-average F1-score represents the combined classification performance across all artery positions. Using the default threshold of 0.500, the per-class F1-scores were 0.8046 for the intraosseous position, 0.0000 for the superficial position, and 0.6323 for the intrasinus position, with an overall micro-average F1-score of 0.8157. When lowering the uniform threshold to 0.452, the F1-score slightly decreased for the intraosseous position to 0.8002 and increased for the intrasinus position to 0.6488, while the superficial position remained unclassified at 0.0000. The overall micro-average F1-score slightly increased to 0.8193. Class-specific thresholds were then applied concurrently, using 0.515 for the intraosseous position, 0.411 for the superficial position, and 0.452 for the intrasinus position. This approach improved the per-class F1-scores to 0.8153 for intraosseous, 0.0164 for superficial, and 0.6470 for intrasinus. As a result, the overall micro-average F1-score reached its highest value of 0.8206, indicating that the class-specific thresholding strategy achieved the best classification performance, as shown in Table 2.

Discussion

The integration of deep learning into medical imaging has become increasingly important, as accurate analysis of anatomical structures plays a key role in diagnosis, treatment planning, and preventing complications [31, 32]. This study marks a significant advancement as the first to utilize a deep learning model for classifying the presence and positional variants of the AAA canal in coronal CBCT images, achieving a high micro F1-score. These results highlight the potential of deep learning for accurately identifying small vascular structures, which could improve clinical decision-making and diagnostic efficiency.

Table 2 The results of the ResNet-18 model performance across different threshold strategies showing per-class F1-scores for each position (I= Intraosseous, S= superficial, and N= Intrasinus) and the overall micro F1-score.

Threshold	F1-score			
	Per-class			Overall micro-average
	I	S	N	
0.500	0.8046	0.0000	0.6323	0.8157
0.452	0.8002	0.0000	0.6488	0.8193
0.452 0.411 0.515	0.8153	0.0164	0.6470	0.8206

Park *et al*. [30] developed a deep learning model to precisely locate the posterior superior alveolar artery (PSAA/AAA) in CBCT images using various 3D networks. However, their study did not address whether their model could detect the absence of the artery, as it primarily focused on detecting and localizing its position. Cases where the PSAA was undetectable due to low image quality or anatomical variations were excluded, suggesting that their analysis was limited to scenarios where the artery was visible rather than determining its presence or absence. In contrast, our study introduces a critical classification step by including frames without the AAA canal to detect artery's presence or absence, which slightly decreased the overall micro F1-score to 0.7. This reduction in performance can be attributed to the inclusion of artery-absent frames, which introduce additional noise and hinder the model's ability to extract relevant features. Nonetheless, this comprehensive approach offers greater clinical relevance by addressing both the detection and precise positioning of the AAA, accounting for realistic variations encountered in clinical practice. Identifying artery absence can reduce bleeding risks and simplify sinus lift surgery, whereas failing to detect an existing artery may lead to unexpected bleeding and surgical complications. Additionally, we successfully classified the positional variations of the AAA canal, enabling clinicians to select the most appropriate preoperative approach and manage unexpected intraoperative bleeding more effectively. Figure 3 illustrates a comparison between expert annotations and model predictions regarding the presence or absence of the artery in different anatomical positions across CBCT frame numbers from two representation patients. The AAA canal typically appears within slices 200–450, confirming this range as corresponding to the posterior maxillary region. This information is highly valuable for clinicians, allowing them to quickly focus on relevant slices, significantly reducing manual inspection time. In Figure 3(a), representing the first patient, the model prediction closely matched expert annotations, accurately classifying the intraosseous artery position with minimal mismatches, and correctly recognizing the absence of superficial or intrasinus positions. However, in the second patient, shown in Figure 3(b), expert annotations revealed a more complex pattern involving all the artery position appearances. In this scenario, the model demonstrates several prediction mismatches (highlighted in orange), notably missing superficial occurrences and exhibiting inaccuracies in identifying intraosseous and intrasinus positions. This detailed comparison underscores regions requiring further clinical verification, helping clinicians quickly pinpoint slices that demand closer inspection while minimizing unnecessary image review. By clearly delineating these critical areas, the proposed approach significantly reduces manual inspection time, enhances diagnostic accuracy, and contributes to safer, more precise surgical planning.

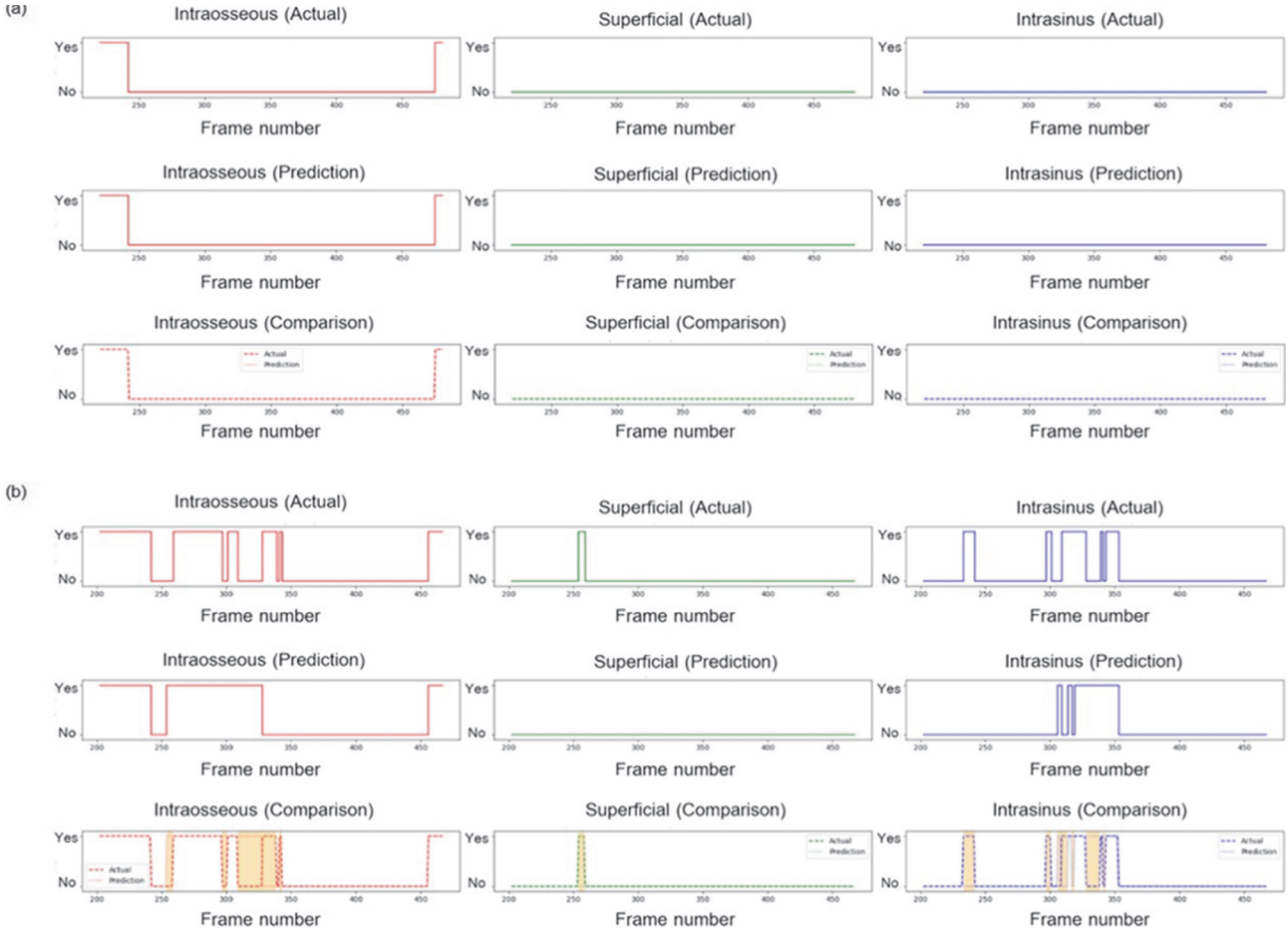

Figure 3 Comparison between actual (expert-annotated) and predicted (model-classified) of alveolar antral artery (AAA) positions across CBCT frames in two patients (a, b). Prediction mismatches highlighted in orange.

A notable challenge encountered in our study was the class imbalance within the dataset, particularly affecting the superficial class, which had significantly fewer samples compared to the other two positions. This finding aligns with existing literature, which reports that the superficial position is naturally less prevalent [5, 33]. The class imbalance likely impacted the F1-score, as deep learning models often struggle with underrepresented classes [34]. This problem can be alleviated by using different threshold adjustment strategies [35]. First, we lowered the default single-threshold to increase recall (sensitivity), aiming to capture more true positives even at the expense of increased false positives for rare classes. As a result, the per-class F1-score demonstrated a slight improvement in the intrasinus classification, however, the model still failed to classify the superficial class and exhibited a minor decline in the classification of intraosseous position. Nonetheless, the overall micro F1-score increased slightly compared to the default threshold. Second, using the class-specific threshold strategy, in which the threshold was lowered specifically for the rare superficial class while being increased for the more abundant classes. This adjustment aimed to recover some false

negative cases in the superficial class with a few sacrificing for false positives. This strategy improved the balance between precision and recall, especially for the superficial class, and led to a small but crucial improvement in the superficial classification, achieving the highest score of both per-class and overall micro F1-score. While this study focused on improving classification performance through threshold lowering and implementing class-specific thresholds, future research could explore the impact of using higher threshold values. Raising the threshold above 0.500 may increase precision by reducing false positives, although this would likely lower recall [35]. Investigating this trade-off would offer clearer insights into the model's sensitivity and help evaluate the stability of the thresholding strategy. Such analysis could enhance the model's reliability and support more informed threshold selection for clinical applications. Additionally, our study incorporated class weighting based on inverse frequency, which helped balance the contribution of each class in the loss function, further enhancing model robustness.

Despite the promising results of our study, which is the first to classify the AAA canal presence in three positions using coronal CBCT images and addresses a previously unexplored clinical challenge, several important limitations should be acknowledged. First, our dataset was limited to 60 patients, which may not fully capture the variety of anatomical variations present in the broader population. Second, analyzing the AAA canal from coronal CBCT images could be challenged. According to the study of previous studies, the average diameter of this artery presented in CBCT image is about 1.0-1.5 mm, making it inherently more difficult to classify [5, 9, 36]. Additionally, as our data was collected from a single hospital without external validation, the model's generalizability to different patient populations and healthcare settings remains uncertain. Furthermore, our study relied on a single deep learning architecture, which may have limited the model's potential performance compared to more advanced or ensemble approaches.

Expanding the dataset and collaborating across multiple centers should be prioritized in future research to enhance the model's reliability, generalizability, and clinical relevance. Although the current classification model effectively identifies AAA canal positions, it lacks spatial localization capabilities, which are critical for guiding surgical planning. Future research should explore object detection models such as YOLO (You Only Look Once) or Faster R-CNN, which are capable of both classifying and localizing anatomical structures [24, 37]. Integrating these models could significantly improve the clinical utility of AI-based detection systems by providing comprehensive spatial information, improving preoperative planning and reducing surgical risks. This study highlights the potential of deep learning in automated vascular classification, making the AAA canal classification more efficient and accurate.

Conclusion

In summary, this study provides the first deep learning-based classification of the presence or absence of the AAA canal positions, making the AAA canal classification more efficient and accurate. Class-specific thresholds improve performance compared to single-threshold method. Our findings lead the way for future advancements in deep learning applications for medical imaging, highlighting the potential of deep learning in medical image analysis.

These advancements could benefit clinicians in diagnosis, treatment planning, and surgery, leading to better patient outcomes.

Acknowledgements

The authors would like to express their sincere gratitude to Mr. Sorawit Piriyapanyaporn, Mr. Pathompum Jirakarnpaisan, and Mr. Phusit Mongkhonwatcharaphun, undergraduate students from the Faculty of Information and Communication Technology, Mahidol University, Salaya Campus, Nakorn Pathom, Thailand, for their valuable contributions to this research. Their efforts in developing the model and assisting in data analysis were instrumental in the success of this study.

References

1. Larsen PE, Kennedy KS. Managing the posterior maxilla with implants using bone grafting to enhance implant sites. ***Oral Maxillofac Surg Clin North Am***. 2019 May;31(2):299-308. doi:10.1016/j.coms.2019.01.002.
2. Molina A, Sanz-Sánchez I, Sanz-Martín I, Ortiz-Vigón A, Sanz M. Complications in sinus lifting procedures: Classification and management. ***Periodontol 2000***. 2022 Feb;88(1):103-115. doi:10.1111/prd.12414.
3. Rosano G, Taschieri S, Gaudy JF, Weinstein T, Del Fabbro M. Maxillary sinus vascular anatomy and its relation to sinus lift surgery. ***Clin Oral Implants Res***. 2011 Jul;22(7):711-715. doi:10.1111/j.1600-0501.2010.02045.x.
4. Danesh-Sani SA, Movahed A, ElChaar ES, Chong Chan K, Amintavakoli N. Radiographic evaluation of maxillary sinus lateral wall and posterior suerior alveolar artery anatomy: A cone-beam computed tomographic study ***Clin Implant Dent Relat Res***. 2017 Feb;19(1):151-160. doi:10.1111/cid.12426.
5. Laovoravit V, Kretapirom K, Pornprasertsuk-Damrongsri S. Prevalence and morphometric analysis of the alveolar antral artery in a group of Thai population by cone beam computed tomography. ***Oral Radiol***. 2021;37(3):452-462. doi:10.1007/s11282-020-00478-3.
6. Fahrettin Kalabalık HA. Evaluation of the alveolar antral artery position in the lateral sinus wall using cone-beam computed tomography. ***Ann Clin Anal Med*** 2020;11(4):330-334. doi: 10.4328/ACAM.20084
7. Zijderveld SA, van den Bergh JP, Schulten EA, ten Bruggenkate CM. Anatomical and surgical findings and complications in 100 consecutive maxillary sinus floor elevation procedures. ***J Oral Maxillofac Surg***. 2008 Jul;66(7):1426-1438. doi:10.1016/j.joms.2008.01.027
8. Jensen SS, Eriksen J, Schiodt M. Severe bleeding after sinus floor elevation using the transcrestal technique: a case report. ***Eur J Oral Implantol***. 2012 Autumn;5(3):287-291.
9. Yang DH, Lee NV. A simple method of managing the alveolar antral artery during sinus lift surgery. ***Int J Otolaryngol Head Neck Surg***. 2021;10:131-146. doi: 10.4236/ijohns.2021.103014.
10. Varela-Centelles P, Loira M, González-Mosquera A, Romero-Mendez A, Seoane J, García-Pola MJ, *et al*. Study of factors influencing preoperative detection of alveolar antral artery by CBCT in sinus floor elevation. ***Sci Rep***. 2020 Jul 2;10(1):10820. doi:10.1038/s41598-020-67644-9.
11. Testori T, Tavelli L, Scaini R, Saibene AM, Felisati G, Barootchi S, *et al*. How to avoid intraoperative and postoperative complications in maxillary sinus elevation. ***Periodontol 2000***. 2023 Jun;92(1):299-328. doi:10.1111/prd.12480.
12. Pimkhaokham A, Aung CMS, Panmekiat S. The study of the alveolar antral artery canal in using cone beam computed tomography. ***M Dent J.*** 2016;37(1):63-69.
13. Ilgüy D, Ilgüy M, Dolekoglu S, Fisekcioglu E. Evaluation of the posterior superior alveolar artery and the maxillary sinus with CBCT. ***Braz Oral Res***. 2013 Sep-Oct;27(5):431-437. doi:10.1590/s1806-83242013000500007.

14. Ketabi AR, Hassfeld S, Lauer HC, Piwowarczyk A. Comparative diagnosis of the alveolar antral artery canal in the lateral maxillary sinus wall in corresponding panoramic radiography and cone-beam computed tomography. ***Int J Implant Dent***. 2023 Sep 19;9(1):30. doi:10.1186/s40729-023-00497-9.
15. Kqiku L, Biblekaj R, Weiglein AH, Kqiku X, Städtler P. Arterial blood architecture of the maxillary sinus in dentate specimens. ***Croat Med J***. 2013 Apr;54(2): 180-184. doi:10.3325/cmj.2013.54.180.
16. Solar P, Geyerhofer U, Traxler H, Windisch A, Ulm C, Watzek G. Blood supply to the maxillary sinus relevant to sinus floor elevation procedures. ***Clin Oral Implants Res***. 1999 Feb;10(1):34-44. doi:10.1034/j.1600-0501.1999.100105.x.
17. Ossowska A, Kusiak A, Świetlik D. Artificial Intelligence in dentistry-narrative review. ***Int J Environ Res Public Health***. 2022 Mar 15;19(6):3449. doi: 10.3390/ijerph 19063449.
18. Anaya-Isaza A, Mera-Jiménez L, Zequera-Diaz M. An overview of deep learning in medical imaging. ***Inform Med Unlocked***. 2021;26:100723. doi:10.1016/j.imu.2021.100723.
19. Xu W, Fu YL, Zhu D. ResNet and its application to medical image processing: Research progress and challenges. ***Comput Methods Programs Biomed***. 2023 Oct;240:107660. doi:10.1016/j.cmpb.2023.107660.
20. He K, Zhang X, Ren S, Sun J. Deep residual learning for image recognition. ***2016 IEEE Conference on Computer Vision and Pattern Recognition (CVPR)***. Las Vegas, NV, USA, 2016, pp.770-778, doi: 10.1109/CVPR.2016.90.
21. Yang Y, Zhang L, Du M, Bo J, Liu H, Ren L, *et al.* A comparative analysis of eleven neural networks architectures for small datasets of lung images of COVID-19 patients toward improved clinical decisions. ***Comput Biol Med***. 2021 Dec;139:104887. doi:10.1016/j.compbiomed.2021.104887.
22. Huang G, Liu Z, Maaten LVD, Weinberger KQ, editors. Densely connected convolutional networks. ***2017 IEEE Conference on Computer Vision and Pattern Recognition (CVPR)***. Honolulu, USA, 2017, pp.4700-4708. doi.org/10.1109/CVPR.2017.243
23. Wu Z, Zhuo R, Liu X, Wu B, Wang J. Enhancing surgical decision-making in NEC with ResNet18: a deep learning approach to predict the need for surgery through x-ray image analysis. ***Front Pediatr***. 2024 Jun 4;12:1405780. doi:10.3389/fped.2024.1405780.
24. Jiang T, Lu Z, Hu X, Zeng L, Ma X, Huang J, *et al*. Deep learning multi-label tongue image analysis and its application in a population undergoing routine medical checkup. ***Evid Based Complement Alternat Med***. 2022 Sep 29;2022:3384209. doi:10.1155/2022/3384209.
25. Kwak GH, Kwak EJ, Song JM, Park HR, Jung YH, Cho BH, *et al*. Automatic mandibular canal detection using a deep convolutional neural network. ***Sci Rep***. 2020 Mar 31;10(1):5711. doi:10.1038/s41598-020-62586-8.
26. Jaskari J, Sahlsten J, Järnstedt J, Mehtonen H, Karhu K, Sundqvist O, *et al.* Deep learning method for mandibular canal segmentation in dental cone beam computed tomography volumes. ***Sci Rep.*** 2020 3 Apr;10(1):5842. doi:10.1038/s41598-020-62321-3.
27. Choi H, Jeon KJ, Kim YH, Ha E-G, Lee C, Han S-S. Deep learning-based fully automatic segmentation of the maxillary sinus on cone-beam computed tomographic images. ***Sci Rep***. 2022 Aug 17;12(1): 14009. doi:10.1038/s41598-022-18436-w.
28. Rahpeyma A, Khajehahmadi S. Alveolar antral artery: review of surgical techniques livolving this anatomic structure. ***Iran J Otorhinolaryngol***. 2014; 26(75):73-78.
29. Maridati P, Stoffella E, Speroni S, Cicciù M, Maiorana C. Alveolar antral artery isolation during sinus lift procedure with the double window technique. ***Open Dent J***. 2014 May30;8:95-103. doi:10.2174/1874210601408010095.
30. Park JA, Kim D, Yang S, Kang JH, Kim JE, Huh KH, *et al*. Automatic detection of posterior superior alveolar artery in dental cone-beam CT images using a deeply supervised multi-scale 3D network. ***Dentomaxillofac Radiol***. 2024 Jan 11;53(1):22-31. doi:10.1093/dmfr/twad002.
31. Putra RH, Doi C, Yoda N, Astuti ER, Sasaki K. Current applications and development of artificial intelligence for digital dental radiography. ***Dentomaxillofac Radiol***. 2022 Jan1;51(1):20210197. doi:10.1259/dmfr.20210197.

32. Schwendicke F, Samek W, Krois J. Artificial intelligence in dentistry: chances and challenges. ***J Dent Res***. 2020 Jul;99(7):769-774. doi:10.1177/0022034520915714.
33. Staněk J, Machálková K, Staňková M, Zapletalová J, Kocurová T. Alveolar antral artery: cone beam computed tomography study and clinical context. ***PeerJ***. 2023 Nov 30;11:e16439. doi:10.7717/peerj.16439.
34. Luque A, Carrasco A, Martín A, de las Heras A. The impact of class imbalance in classification performance metrics based on the binary confusion matrix. ***Pattern Recognit***. 2019 Jul;91:216-231. doi:10.1016/j.patcog.2019.02.023.
35. Saito T, Rehmsmeier M. The precision-recall plot is more informative than the ROC plot when evaluating binary classifiers on imbalanced datasets. ***PLoS One***. 2015 Mar4;10(3):e0118432. doi:10.1371/journal.pone.0118432.
36. Benjaphalakron N, Jansisyanont P, Chuenchompoonut C, Kiattavorncharoen S. Evaluation of the posterior superior alveolar artery and related factors using cone beam computed tomography images. ***JDAT*** 2021;71:35-43.
37. Ragab MG, Abdulkadir SJ, Muneer A, Alqushaibi A, Sumiea EH, Qureshi R, *et al.* A comprehensive systematic review of YOLO for medical object detection (2018 to 2023). ***IEEE Access*** 2024 Apr.;12:57815 - 57836. doi: *10.1109/ACCESS.2024.3386826.*